Supplementary Information

Study of Charge Transition-Driven Resistive Switching Mechanism in TiO_2-based Random Access Memory via Density Functional Theory

Taeyoung Jeong[1,2], In Won Yeu[1], Kun Hee Ye[1,2], Seungjae Yoon[1,2], Dohyun Kim[1,2], Cheol Seong Hwang[*,2], and Jung-Hae Choi[*,1]

[1]*Electronic Materials Research Center, Korea Institute of Science and Technology, Seoul 02792, Korea*

[2]*Department of Materials Science and Engineering and Inter-University Semiconductor Research Center, Seoul National University, Seoul 08826, Korea*

**Corresponding author;*

Tel.: +82 2 880 7535. Fax: +82 2 884 1413

E-mail address: cheolsh@snu.ac.kr *(C. S. Hwang)*

Tel.: +82 2 958 5488. Fax: +82 2 958 6658

E-mail address: choijh@kist.re.kr *(J.-H. Choi)*

Supplementary note 1

Methodology to determine the ION of each V_O

This supplementary note describes the approach for estimating the individual oxidation number (ION) of an oxygen vacancy (V_O) using Bader charge (BC) distribution. This approach is based on the observation that the charge of an oxygen vacancy (V_O) is highly localized onto the three neighboring Ti ions. Fig. S2a-c show the BC distributions of Ti ions in the presence of an isolated V_O with ION of 0, +1, and +2, respectively, where x-axes indicate Ti ions in the 3×3×6 rutile TiO_2 supercell. The Ti ions with coordination numbers (CNs) of 5 and 6 correspond to the neighboring and non-neighboring Ti ions to V_O, respectively. The green dashed lines represent the average BC value of the 6-coordinated Ti ions in each case, while the red dashed lines indicate the average BC value of the Ti ions in a perfect cell for comparison. Note that the BC values of three 5-coordinated Ti ions significantly changed by both the presence of V_O and its charge state, while those of the other 6-coordinated Ti ions remained unvaried, clearly showing the strong charge localization nature of V_O in rutile TiO_2. Therefore, the BC value of neighboring Ti ions can be used for estimating the ION of V_O.

Two key parameters were chosen for estimating the IONs of V_Os in arbitrary configuration: (1) ΣBC, defined as the sum of BC values of three neighboring Ti ions surrounding a certain V_O. This parameter quantifies the extent to which the electrons of the V_O are localized to the three neighboring Ti ions, with a lower ΣBC value indicating more localized electrons. (2) CNs of the three neighboring Ti ions. As described in Section **A** of the main text, the charge localization effect of the Ti ion varies according to its CN. Hence, V_Os were classified into three cases according to the CNs of the three neighboring Ti ions: *CN555* case when all three Ti ions are 5-coordinated; *CN455* case when one of the neighboring Ti ions is 4-coordinated, while the

other two are 5-coordinated; *CN445* case when two of the neighboring Ti ions are 4-coordinated, and the other is 4-coordinated. The other possibilities, such as the *CN444* case, where all three Ti ions are 4-coordinated, were neglected as they did not occur in this study. In the remainder of this note, the ΣBC to ION relationship for each case will be established, and these relationships will be applied to explain the resistive switching process, as described in Section **C** of the main text.

1. ΣBC to ION relationship for *CN555*

A supercell containing an isolated V_O, as shown in Fig. S2d, is the most straightforward system of *CN555*. In this system, the ION of V_O is the same as the total charge of the supercell. The ΣBC values for an isolated V_O^0, V_O^{1+}, and V_O^{2+} were calculated using the BC distributions in Fig. S2a-c and are represented by the black squares in Fig. S2e. Notably, the ΣBC and ION exhibited a nearly linear relationship. To validate this relationship, the ΣBC was additionally calculated for an isolated $V_O^{0.5+}$ and $V_O^{1.5+}$, as represented by the open squares in Fig. S2e. They aligned well with the linear relationship between ΣBC and ION, meaning that the ION of an isolated V_O can be estimated by this ΣBC to ION relationship.

However, to achieve the goal, this ΣBC to ION relationship should be applied to arbitrary V_Os (multiple V_Os contained in a supercell) in the *CN555* case, as well as an isolated V_O. The colored squares in Fig. S2e show the ΣBC to ION relationship when two V_Os exist at a distance of 4.42 Å or more (see the legend) in a supercell. For distances closer than 4.42 Å, a 4-coordinated Ti ion is formed, addressed in the next section. The two V_O-sites in a supercell are equivalent, irrespective of the distance between the two V_Os since all O-sites in rutile are

equivalent. Hence, the IONs of the two V_Os are equal to half of the total charge of the supercell. It should be noted that, compared to the ΣBC to ION relationship for an isolated V_O (black squares), the relationship remains consistent regardless of the presence of another adjacent V_O and its location. This finding means that the ΣBC value is hardly affected by other nearby V_O, and this characteristic is confirmed by the electron cloud diagram. Fig. S2f shows electron clouds for two V_O^0s separated by 4.42 Å. Despite the proximity between the two V_O^0s, the electron clouds remain intact compared to the electron cloud for an isolated V_O^0, shown in Fig. S2d. This independence of electron clouds is due to the highly localized nature of electrons of V_O to the neighboring Ti ions, ensuring the applicability of the ΣBC to ION relationship in Fig. S2e to arbitrary V_O in the *CN555* case.

2. ΣBC to ION relationship for *CN455* and *CN445*

Fig. S3a and b show V_O configurations used to examine the ΣBC to ION relationship for *CN455* and *CN445* cases, respectively. The symmetrically equivalent V_O-sites in these supercells enable the calculation of the ION of V_O by dividing the total charge of the supercell by the number of V_O. These are the only ones allowing ION calculation for V_Os in *CN455* and *CN445* cases, as V_O-sites in other configurations are not equivalent. Fig. S4a-c and S4d-f show BC distributions for the *CN455* and *CN445* cases, respectively. The red and green dashed lines have the same meaning as in Fig. S2. Notably, the 4-coordinated Ti ions manifest a more substantial charge localization effect than the 5-coordinated Ti ions. Since the electron clouds for V_Os in *CN455* or *CN445* cases are more localized to the three neighboring Ti ions than those in the *CN555* case, the presence of other nearby V_O will barely affect the ΣBC value,

similar to the *CN555* case.

Finally, ΣBC to ON relationships for the *CN455* and *CN445* cases are calculated, as shown in Fig. S5. Here, all physically feasible IONs which ensure that the electron count of the supercell remains an integer are considered; accordingly, a total of five IONs (0, +0.5, …, +2) are considered for the *CN455* case, while a total of thirteen IONs (0, +1.67, …, +2) are considered for the *CN445* case.

3. Summary and validation

In summary, the ION of each V_O is calculated in the following sequences: (1) the BC distribution in the supercell is obtained using the open-source code by the Henkelman group with the default setting;[1] (2) the ΣBC for each V_O is calculated. Here, for the compensation of the marginal influence of the delocalized charge, the difference between the average BC of the 6-coordinated Ti ions and the BC of the Ti ion in the perfect rutile TiO_2 cell is subtracted from the BC values of the 4- or 5-coordinated Ti ions; (3) the ION of each V_O is calculated via linear interpolation or extrapolation based on the ΣBC to ON relationship in Fig. S5.

In order to validate the accuracy of the approach, the sum of IONs obtained from our approach is compared with the actual total charge of the supercell, as shown in Table S1. Ideally, these two values should be the same. The approach produced an error of less than 3%, indicating that our approach successfully approximates the IONs. This accuracy suffices for the goal to reveal the tendency of how the IONs change during the switching operation of RRAM.

It should be noted that this methodology relies heavily on both the charge localization nature of V_O and the high permittivity of rutile TiO_2. The exceptionally high

permittivity (over 100) screens the interaction between V_Os, enabling the application of the ΣBC to ON relationship to each V_O irrespective of the presence of other adjacent V_Os. Accordingly, a sizable error can be involved for materials with relatively lower permittivity, such as HfO_2 and Ta_2O_5. Conversely, the methodology likely holds for materials with extremely high permittivity, like $SrTiO_3$, although thorough verification is necessary.

Supplementary note 2

Oxygen ion exchange at Ti/TiO_2 interface

For the simulation of the oxygen ion exchange at the Ti/TiO_2 interface, the interface was constructed by stacking the $(10\bar{1}0)$ plane of hexagonal Ti and the (100) plane of rutile TiO_2, as shown in Fig. S11a. The in-plane lattice mismatches were calculated to be 1.27% and -4.63%. To simulate the oxygen ion exchange reaction at the interface, one oxygen ion was moved from the TiO_2 to an interstitial site in the Ti electrode, as depicted by an orange circle in Fig. S11b. The interstitial site was obtained from Pydefect, an open-source Python package.[6] The climbing NEB (cNEB) calculations were conducted to obtain the energetics and kinetic barrier of the exchange reaction. The cNEB calculations for the Frenkel pair generation in bulk TiO_2 were also conducted for comparison. The images were stabilized until the forces were less than 0.05 eV/Å, and the results are shown in Fig. S12. The energy gain (ΔE) and activation energy (E_a) for the Frenkel pair generation in bulk TiO_2 were found to be 5.36 eV, meaning that the formation of V_O-and-O_i (interstitial oxygen) pair in bulk TiO_2 is highly unfavorable. In contrast, for oxygen ion exchange at the interface, ΔE and E_a were calculated to be -1.95 eV and 1.01 eV, respectively, suggesting that the exchange reaction is spontaneous ($\Delta E < 0$) and likely to occur due to the relatively low E_a. Consequently, V_Os are more readily generated at the interface than in the bulk region.

Supplementary note 3

Influence of interaction between V_Os on V_O formation

To comprehend the influence of interaction between V_Os on the V_O formation, a V_O-pair with a separation distance of 3.88 Å was considered, and the transition level diagram (TLD) for the V_O-pair was calculated, as shown in Fig. S13. The TLD for an isolated V_O (identical to Fig. 5b of the main text) is shown together for comparison. The V_O^0s are preferred near the Ti electrode for both cases, but the formation energy (E_f) of the V_O^0-pair (0.67 eV/V_O) is considerably lower than that of an isolated V_O^0 (1.08 eV/V_O). (Here, the influence of the Ti/TiO_2 interface was not considered) This finding suggests that the generation of V_O^0s is facilitated near the existing V_O^0s. Conversely, a V_O^{2+}-pair is unstable across all the Fermi level range, implying that an existing V_O^{2+} suppresses additional generation of V_O^{2+}s nearby. Therefore, V_O^{2+}s will be sparsely distributed around the Pt electrode. On the other hand, an isolated V_O^{1+} is not preferred throughout the Fermi level range, but the V_O^{1+}-pair becomes predominant in the middle range of ε_f. It should be noted that, in the middle range of ε_f, the V_O^{1+}-pair is energetically more stable than separated V_O^0 and V_O^{2+}. Hence, the V_O^{1+}-pair can be formed by pairing the isolated V_O^0 and V_O^{2+}. These results are consistent with the cohesive energy analyses in Section **A** of the main text.

Supplementary Figures

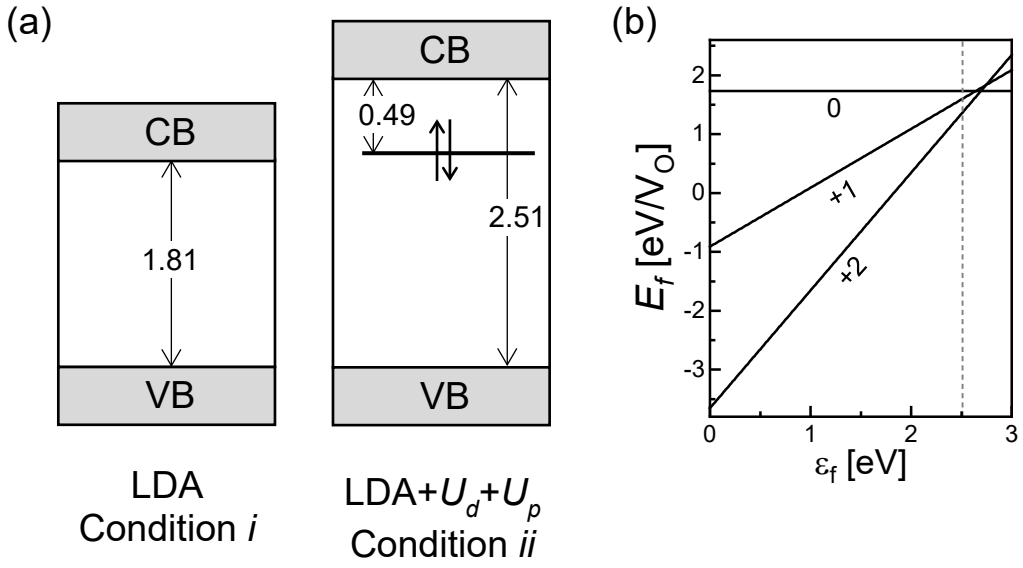

Fig. S1 (a) Band diagrams of a 3×3×6 rutile TiO_2 supercell containing one V_O obtained by conventional LDA calculation (left panel; condition *i*) and by LDA+U_d+U_p calculation (U_d = 4.0 eV, U_p = 9.0 eV) (right panel; condition *ii*). The locations of CBM, VBM, and the defect states are sampled at Γ-point based on the fact that TiO_2 has a direct bandgap of Γ to Γ. The calculated bandgap is 2.51 eV by condition *ii*, which is closer to the experimental bandgap of 3.0 eV than that obtained by condition *i*, 1.81 eV. By condition *ii*, the defect state of V_O^0 is located at 0.49 eV below the CBM, showing a feasible agreement with an experimental value of 0.7 eV.[2] By condition *i*, no defect state exists within the bandgap. (b) Transition level diagram (TLD) of an isolated V_O obtained by the condition *ii*. Note that condition *ii* is set to the previous HSE and DFT+GW studies to ensure accuracy.[3,4] A 2×2×3 rutile supercell is employed, and the chemical potential of an oxygen atom (μ_O) is obtained from the equilibrium condition between TiO_2 and Ti_2O_3. The μ_O in this study, -3.98 eV, is very close to that from the HSE ($\mu_O = -4.07$ eV) and the DFT+GW ($\mu_O = -3.99$ eV) studies. The dashed line at $\varepsilon_f = 2.51$ eV indicates the CBM obtained by condition *ii*, but the range of ε_f was expanded to the experimental band gap (3.0 eV) for comparison. The TLD by condition *ii* also shows feasible agreements with the two previous studies in terms of formation energy (E_f). In addition, the y-intercepts ($\varepsilon_f = 0$) for V_O^0, V_O^{1+}, and V_O^{2+} are 1.73 eV, -0.91 eV, and -3.65 eV, respectively, showing agreement with those for the HSE study (1.69 eV, -1.30 eV, and -4.46 eV) and the DFT+GW study (1.82 eV, -0.68 eV, and -3.67 eV). Consequently, condition *ii* provides reliable defect states and the E_f of V_O^{q+}, which are crucial in this study.

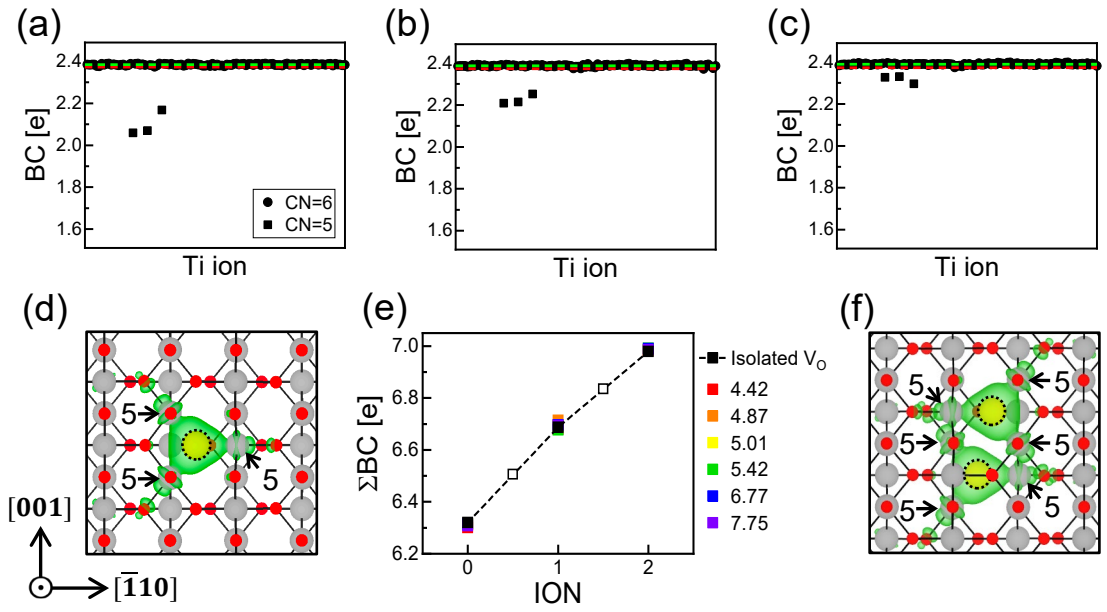

Fig. S2 Bader charge (BC) distributions on Ti ions when an isolated (a) V_O^0, (b) V_O^{1+}, and (c) V_O^{2+} exists in a 3×3×6 rutile TiO_2 supercell, respectively. The x-axes indicate Ti ions in the 3×3×6 rutile TiO_2 supercell. The red dashed lines represent the BC value of the Ti ion in perfect rutile TiO_2, while the green dashed lines represent the average BC value of the 6-coordinated Ti ions in each case. (d) Electron cloud (partial charge density diagram for the defect states) for an isolated V_O^0 (isosurface = 0.005 e/Å). The 5-coordinated Ti atoms are indicated by the arrows. (e) Changes in $\sum BC$ according to ION when an isolated V_O^{q+} $(q = 0, +1, +2)$ exists (black squares) and when two V_O^{q+}s exist at a certain distance from each other (colored squares). The open squares for IONs of +0.5 and +1.5 also show the relationship between $\sum BC$ and ON. (f) Electron clouds for two V_O^0 s with a distance of 4.42 Å (isosurface = 0.005 e/Å). The 5-coordinated Ti ions are indicated by the arrows. For (d) and (f), the grey, red, and yellow circles indicate Ti, O, and V_O, respectively, and this color notation is maintained throughout this study.

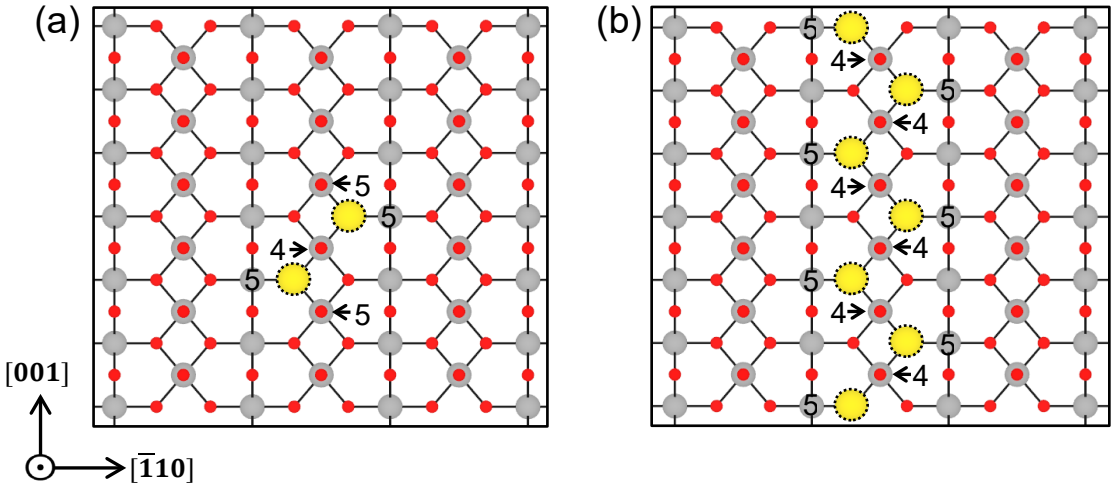

Fig. S3 (a) Atomic structure of the supercell employed for the *CN455* case. Two V_Os are located at the diagonal sites of the equatorial plane of the Ti-O octahedron with a distance of 3.88 Å. (b) Atomic structure of the supercell employed for the *CN445* case, which is the CF structure in this study. The numbers indicate the CN of each Ti ion. Note that the V_O-sites within these two supercells are symmetrically equivalent, so the IONs of V_Os should be the same.

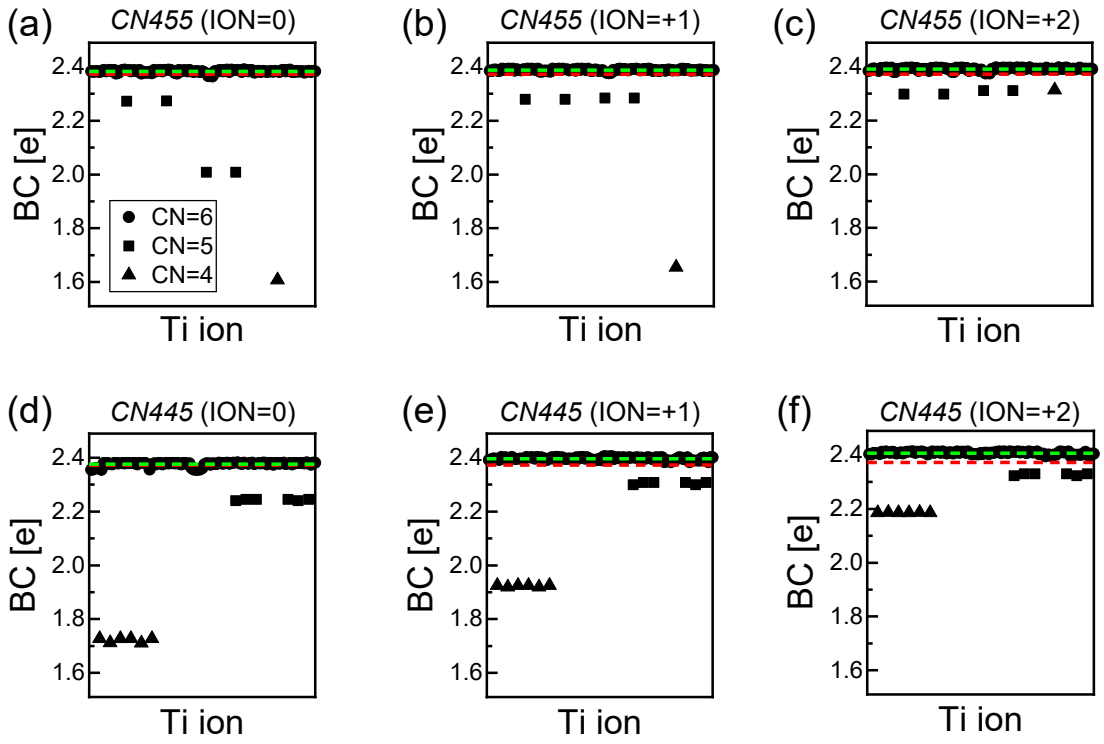

Fig. S4 BC distribution for the *CN455* when the IONs of V_Os are (a) 0, (b) +1, and (c) +2. BC distribution for the *CN445* when the IONs of V_Os are (d) 0, (e) +1, and (f) +2. The red dashed line represents the BC value of the Ti ion in perfect rutile TiO_2, while the green dashed line represents the average BC value of the 6-coordinated Ti ions in each case. The x-axes indicate Ti ions in the 3×3×6 rutile TiO_2 supercell.

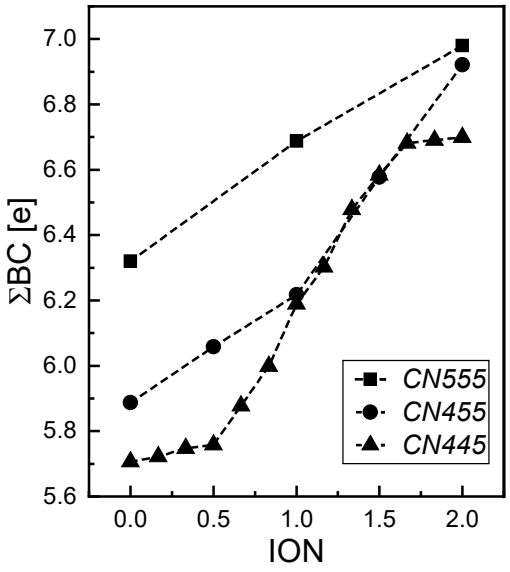

Fig. S5 ∑BC to ION relationship according to the CNs of the three adjacent Ti atoms.

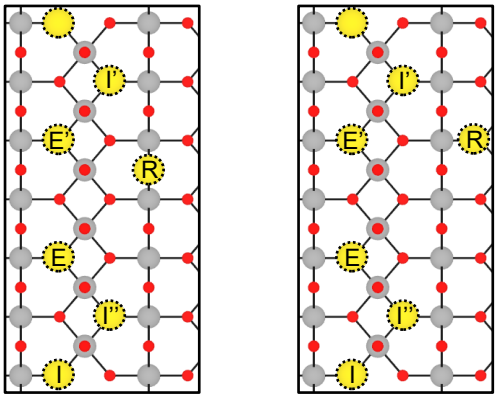

Fig. S6 Schematic illustration of the labels in Table S1. The topmost V_O is the same as the bottom V_O marked by 'I' due to the periodic boundary condition.

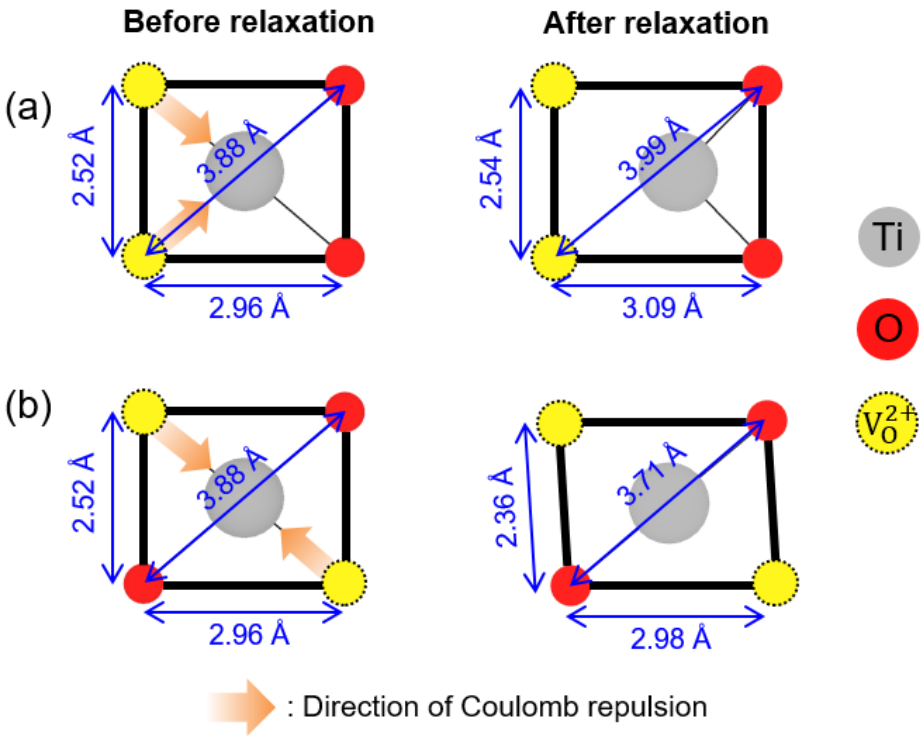

Fig. S7 Equatorial planes of Ti-O octahedrons before and after relaxation when two V_O^{2+}s are separated by (a) 2.52 Å and (b) 3.88 Å. The solid rectangle and dashed lines indicate the equatorial plane and the vertical axis of the Ti-O octahedron, respectively. In (a), the central Ti ion can readily move away from the V_O^{2+}s in the direction of the vector sum of two Coulomb repulsions. In (b), on the contrary, two symmetric Coulomb repulsions cancel out, hindering the central Ti ion from being sufficiently displacing.

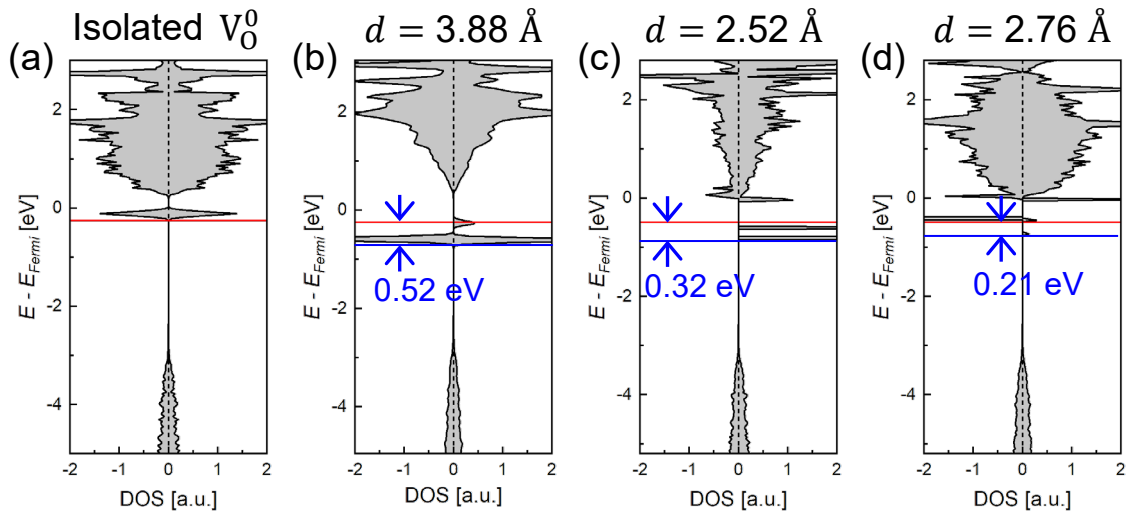

Fig. S8 (a) Atom-resolved electronic density of states (DOS) obtained by projection onto a 5-coordinated Ti ion (Ti ion adjacent to V_O^0) when the supercell contains an isolated V_O^0. The defect state is 0.49 eV below CBM, as shown in Fig. S1. Atom-resolved DOSs obtained by projection onto the 4-coordinated Ti ion when the supercell contains two V_O^0s separated by (b) 3.88 Å, (c) 2.52 Å, and (d) 2.76 Å, respectively. In (b), the defect states are the deepest, resulting in the minimum of the E_{coh}. In (d), the deepest defect state is 0.21 eV deeper than those induced by an isolated V_O^0, but its magnitude of DOS is negligible. On the other hand, its second deepest defect state, showing the largest magnitude of DOS, has almost the same depth as the defect states induced by an isolated V_O^0, resulting in nearly zero E_{coh}, as shown in Fig. 2a of the main text.

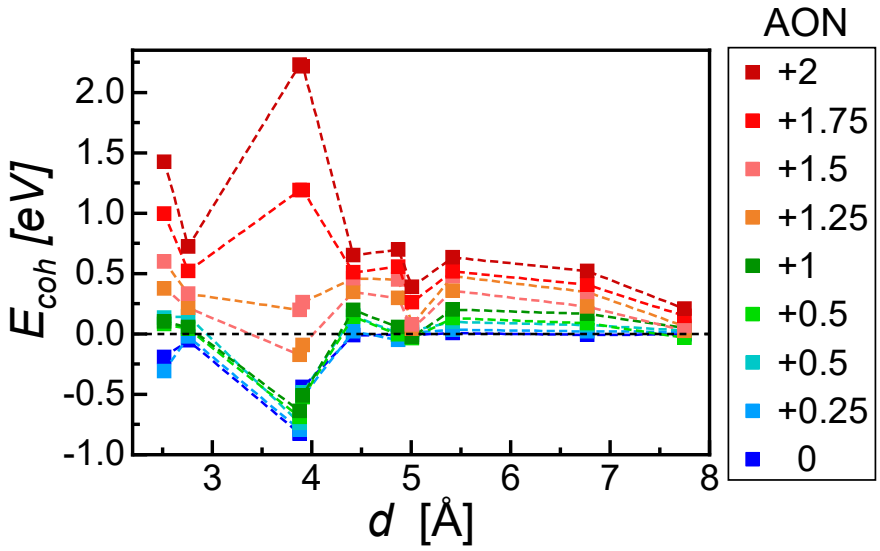

Fig. S9 E_{coh} as a function of the distance between two V_O^{q+}s, considering fractional oxidation number. Although the AONs of +0.25, +0.75, +1.25, and +1.75 are infeasible since the number of electrons contained in the supercell is not an integer, they are taken into account to ensure the trend in E_{coh} according to the oxidation number. The AONs ranging from 0 to +1 show similar attractive E_{coh} trends, while the AONs exceeding +1 exhibit significant increases in E_{coh}, especially at distances of 3.88 Å and 3.91 Å.

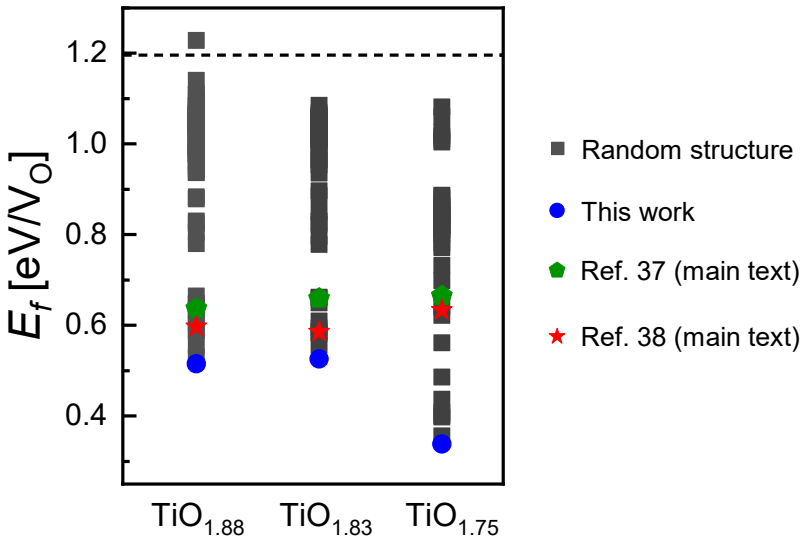

Fig. S10 E_f distributions for various configurations in three compositions of $TiO_{1.88}$, $TiO_{1.83}$, and $TiO_{1.75}$, including two CF structures previously suggested (green pentagons and red stars) for the AON of 0. The dashed lines indicate the E_f of an isolated V_O^0. See Table S2 for information on the random structures employed in these calculations.

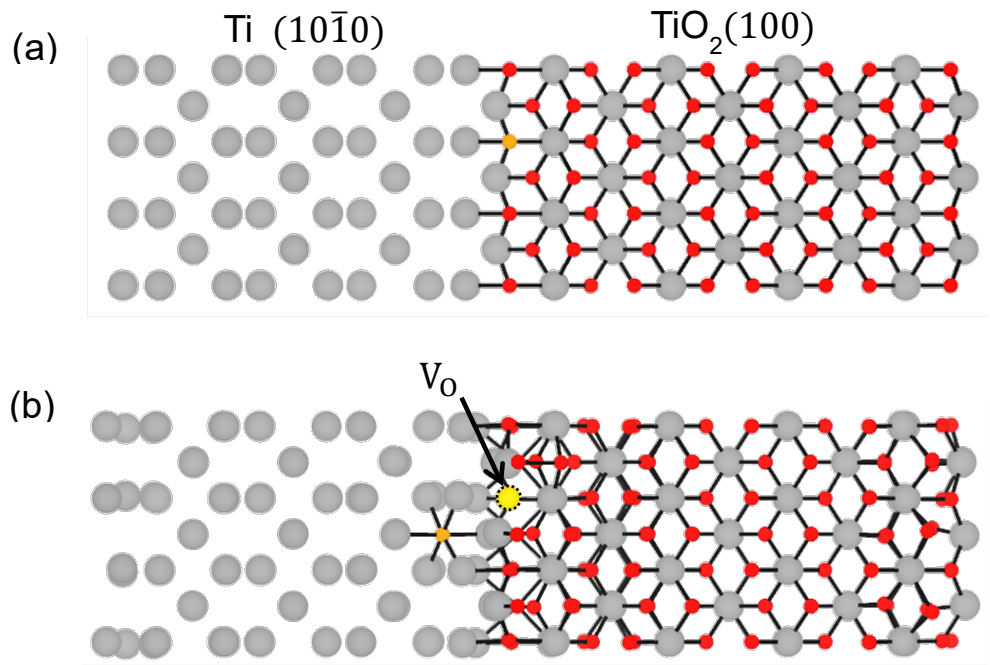

Fig. S11 Atomic structures of the Ti/TiO_2 interface. (a) clean and (b) after oxygen ion exchange. The grey and red circles represent the Ti ions and O ions, respectively. The moving oxygen ion is represented by an orange circle. The dotted yellow circle indicates the generated oxygen vacancy due to the exchange.

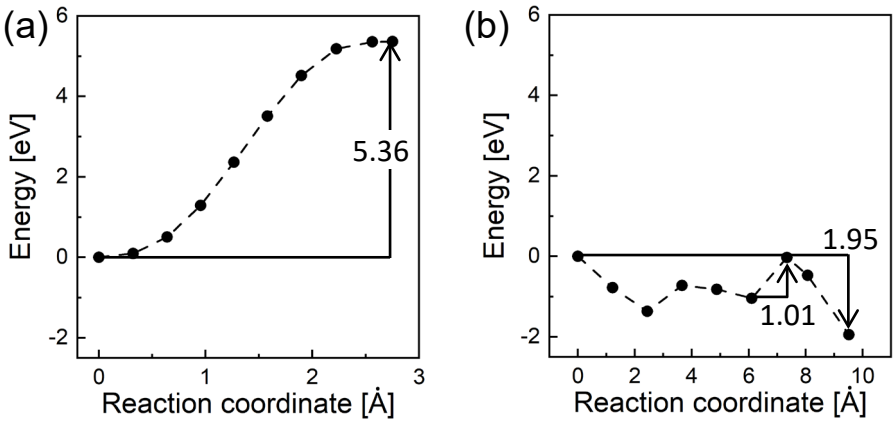

Fig. S12 Energy gain (ΔE) and activation energy (E_a) for (a) Frenkel pair generation and (b) oxygen ion exchange at the Ti/TiO_2 interface.

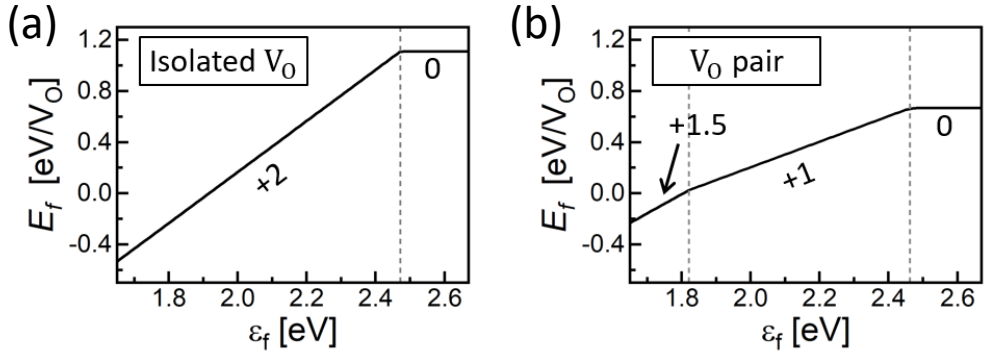

Fig. S13 TLDs for (a) an isolated V_O and (b) a V_O-pair (right panel). The x-axes represent the Fermi level with respect to the valance band maximum of TiO_2. The left and right ends of the x-axes correspond to the region near the Pt electrode and the Ti electrode, respectively. The numbers indicate the preferred average oxidation number (AON) of V_Os.

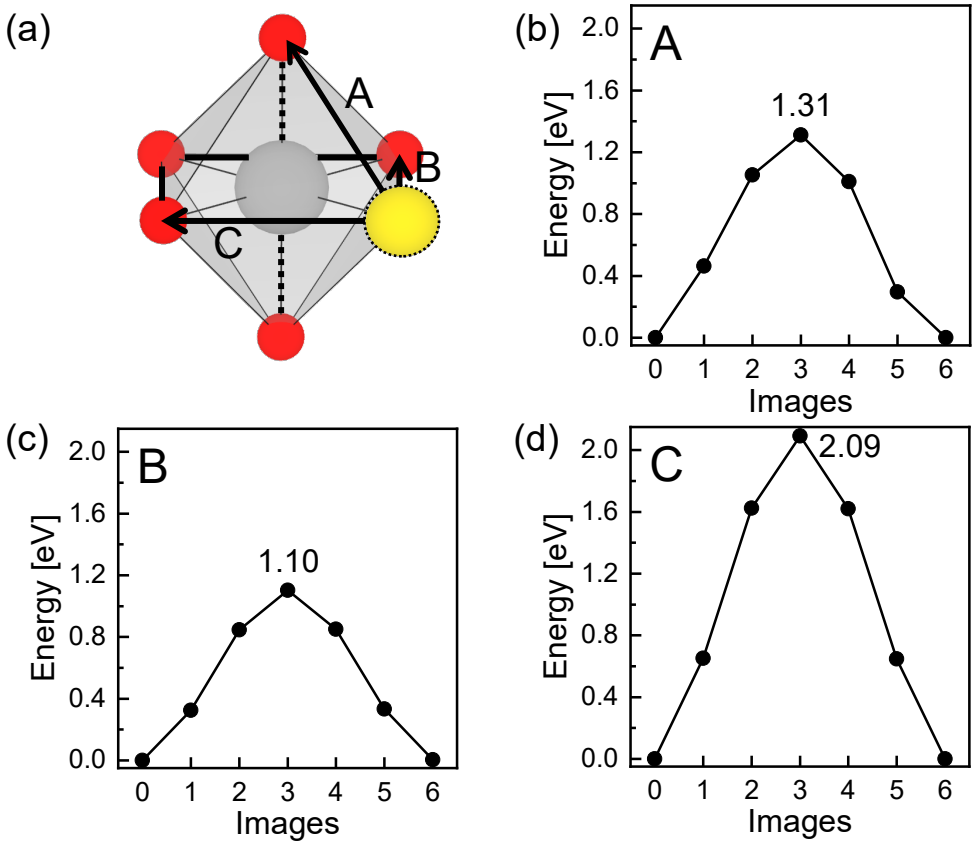

Fig. S14 (a) Atomic structure of the Ti-O octahedron. Three paths of V_O^{2+} diffusion are denoted by A, B, and C. The bold lines and dashed lines represent the equatorial plane and the vertical axis of the Ti-O octahedron, respectively. The length of each path is the same as Fig. 2b of the main text. The cNEB profiles for (b) path A, (c) path B, and (d) path C, respectively. Although path B exhibits the lowest activation barrier, the motion of the V_O^{2+} is confined to one edge of the Ti-O octahedron if only path B is considered. Furthermore, path C can be divided into two sequential paths of A. Consequently, the diffusion barrier of V_O^{2+} is 1.31 eV.

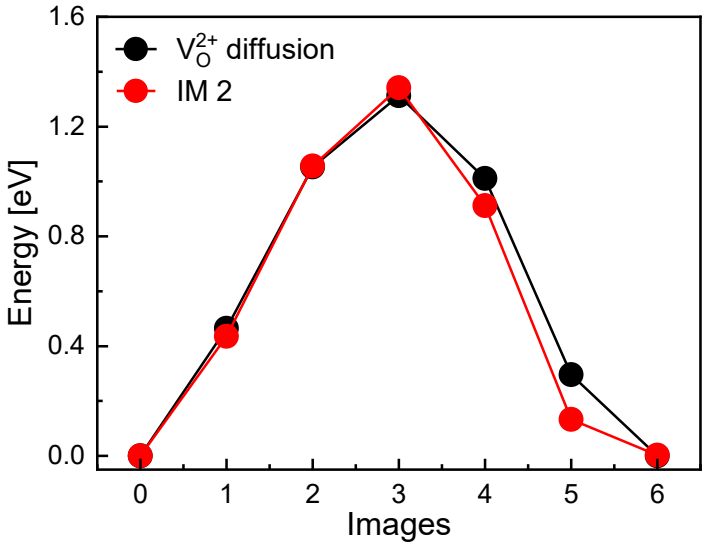

Fig. S15 Comparison of the cNEB profiles for the IM 2 and the V_0^{2+} diffusion.

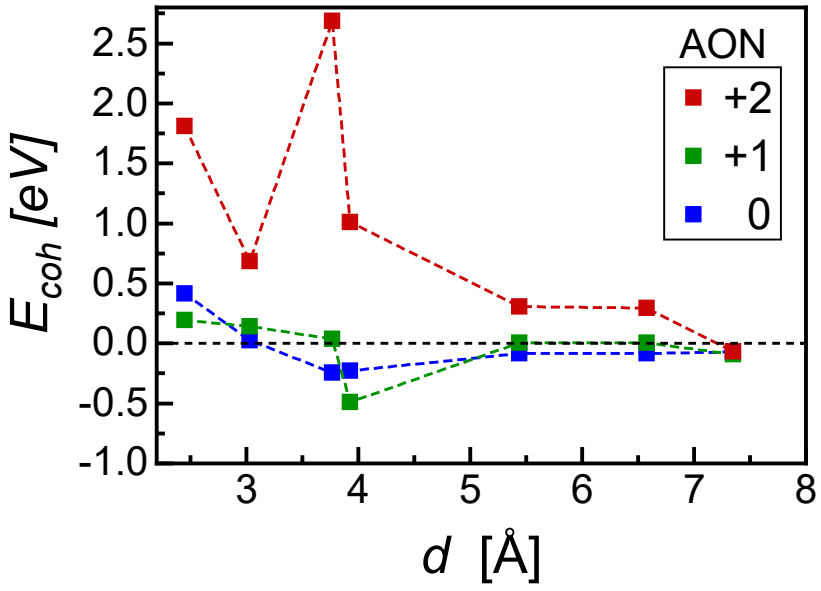

Fig. S16 E_{coh} as a function of the distance between two V_0^{q+}s anatase TiO_2, showing a similar tendency with rutile TiO_2 in Fig. 2a.

Supplementary Tables

Table S1 Estimated IONs of V_Os for the processes described in Section **C** of the main text. See Fig. S6 for a description of the labels. The errors are calculated by comparing the calculated total ON and the actual total charge of the supercell.

Process		**IM 1 (+1.33)**		**IM 2 (+1.33)**		**IM 1 (+1.17)**		**IM 2 (+1.17)**		**e^--injection**	
Label	Case	∑BC	ION	∑BC	ION	∑BC	ION	∑BC	ION	∑BC	ION
I'	*CN445*	6.20	+1.01	6.23	+1.06	5.89	+0.69	5.97	+0.80	5.82	+0.59
E'	*CN455*	6.61	+1.55	6.55	+1.47	6.25	+1.04	6.19	+0.90	6.20	+0.95
R	*CN555*	6.99	+2.03	7.00	+2.07	6.99	+2.02	7.00	+2.07	6.70	+1.03
E	*CN455*	6.57	+1.49	6.60	+1.53	6.58	+1.51	6.59	+1.52	6.20	+0.95
I"	*CN445*	6.14	+0.95	6.19	+1.00	6.15	+0.97	6.17	+0.98	5.84	+0.62
I	*CN445*	6.11	+0.93	6.15	+0.96	6.04	+0.87	5.97	+0.80	6.02	+0.86
Total ON		+7.96		+8.09		+7.09		+7.20		+4.99	
Actual total charge		+8		+8		+7		+7		+5	
Error [%]		**-0.5**		**1.2**		**1.3**		**2.9**		**-0.1**	

Table S2 Detailed information on supercells employed for Fig. S10. All symmetrically different structures are considered by DBmaker in Lattice Configuration Simulation (LACOS) package.[5]

Composition		Supercells	Number of structures
$TiO_{1.88}$	16 Ti, 30 O	1×1×8, 2×1×4, 2×2×2, 4×1×2, 4×2×1, 8×1×1, $\sqrt{2}\times\sqrt{2}\times4$	120
$TiO_{1.83}$	12 Ti, 22 O	1×1×6, 2×1×3, 2×3×1, 3×1×2, 6×1×1, $\sqrt{2}\times\sqrt{2}\times3$	71
$TiO_{1.75}$	8 Ti, 14 O	1×1×4, 1×2×2, 2×2×1, 4×1×1, $\sqrt{2}\times\sqrt{2}\times2$	44
		Total number	235

References

1. G. Henkelman, A. Arnaldsson and H. Jónsson, *Comput. Mater. Sci.* 2006, **36**, 354.
2. V. E. Herich, G. Dresselhaus and H. J. Zeiger, *Phys. Rev. Lett.* 1976, **36**, 1335.
3. A. Janotti, J. B. Varley, P. Rinke, N. Umezawa, G. Kresse and C. G. Van de Walle, *Phys. Rev. B* 2010, **81**, 0852121.
4. A. Malashevich, M. Jain and S. G. Louie, *Phys. Rev. B* 2014, **89**, 075205.
5. M. Chandran, *Comput. Mater. Sci.* 2015, **108**, 192–204.
6. Yu Kumagai, Naoki Tsunoda, Akira Takahashi, and Fumiyasu Oba, *Phys. Rev. Materials* 2021, **5**, 123803.